# Intravascular photoacoustic imaging of exogenously labeled atherosclerotic plaque through luminal blood

Doug Yeager
Andrei Karpiouk
Bo Wang
James Amirian
Konstantin Sokolov
Richard Smalling
Stanislav Emelianov

# Intravascular photoacoustic imaging of exogenously labeled atherosclerotic plaque through luminal blood

Doug Yeager,[a] Andrei Karpiouk,[a] Bo Wang,[a] James Amirian,[b] Konstantin Sokolov,[a,c] Richard Smalling,[b] and Stanislav Emelianov[a,c]
[a]University of Texas at Austin, Department of Biomedical Engineering, Austin, Texas 78712
[b]University of Texas Health Science Center, Division of Cardiology, Houston, Texas 77030
[c]M.D. Anderson Cancer Center, Department of Imaging Physics, Houston, Texas 77030

**Abstract.** Combined intravascular ultrasound and intravascular photoacoustic (IVUS/IVPA) imaging has been previously established as a viable means for assessing atherosclerotic plaque morphological and compositional characteristics using both endogenous and exogenous contrast. In this study, IVUS/IVPA imaging of atherosclerotic rabbit aortas following systemic injection of gold nanorods (AUNRs) with peak absorbance within the tissue optical window is performed. *Ex vivo* imaging results reveal a high photoacoustic signal from localized AUNRs in regions with atherosclerotic plaques. Corresponding histological staining further confirms the preferential extravasation of AUNRs in atherosclerotic regions with compromised luminal endothelium and acute inflammation. The ability to detect AUNRs using combined IVUS and photoacoustic imaging in the presence of luminal saline and luminal blood is evaluated using both spectroscopic and single wavelength IVPA imaging techniques. Results demonstrate that AUNR detection within the arterial wall can be achieved using both methods, even in the case of imaging through luminal blood. © *2012 Society of Photo-Optical Instrumentation Engineers (SPIE).* [DOI: 10.1117/1.JBO.17.10.106016]

Keywords: intravascular imaging; intravascular ultrasound; photoacoustic; gold nanoparticles; gold nanorods; atherosclerosis.

Paper JBO-12303P received May 15, 2012; revised manuscript received Sep. 17, 2012; accepted for publication Sep. 20, 2012; published online Oct. 17, 2012.

## 1 Introduction

Despite significant advances in preventative measures and interventional procedures, cardiovascular disease remains a leading cause of death within industrialized nations. The high mortality rate can be attributed, in part, to an inability to reliably differentiate atherosclerotic plaques which are prone to rupture.[1] These so-called vulnerable plaques initiate at sites with a dysfunctional endothelium and progress over the course of years or decades through a sequence of events involving low density lipoprotein (LDL) infiltration, macrophage accumulation, inflammation, and development of a necrotic lipid-rich core.[2] The ability to locate atherosclerotic lesions and detect functional characteristics associated with plaque progression, such as the extent of endothelial dysfunction, can significantly improve the current ability to determine vulnerability and therefore provide a tool for clinicians when choosing an appropriate treatment.

Current clinical intravascular imaging techniques used for diagnosing atherosclerosis provide a primarily morphological assessment of the vessel. Intravascular imaging modalities such as intravascular ultrasound (IVUS) and optical coherence tomography (OCT) have each been demonstrated to allow differentiation of some relevant tissue types based on variations in their respective backscatter signal intensities;[3] however, each of these imaging techniques has inherent limitations. OCT offers high spatial resolution, on the order of 10 $\mu$m, but provides limited penetration depth and the attenuation of blood necessitates its removal via balloon occlusion or saline flushing during image acquisition.[4] IVUS, on the other hand, may be utilized in the presence of luminal blood and offers sufficient penetration depth to image the full vessel thickness, but with a lower spatial resolution and contrast.

Recently, intravascular photoacoustic (IVPA) imaging has been introduced and characterized.[5,6] Combining clinically approved IVUS imaging with IVPA imaging provides a means of supplementing morphological information obtained from conventional IVUS with a co-registered assessment of atherosclerotic plaque composition. In photoacoustic imaging, absorption of energy from nanosecond duration optical pulses by endogenous tissue chromophores or exogenous contrast agents results in a local thermal expansion of tissues which subsequently generates a pressure wave that is detected and localized using an ultrasound transducer. Because the pressure is generated following optical absorption and localized using an ultrasound receiver, photoacoustic imaging is less sensitive to effects of tissue scattering and the resulting loss of optical coherence. As a result, the achievable penetration depth of photoacoustic imaging is significantly greater than conventional optical techniques.

Furthermore, in the case of IVPA imaging, the contrast between different tissue components is partially dictated by differences in their wavelength-dependent optical absorption. The optical contrast enables differentiation of composition based on unique spectral characteristics of tissues or exogenous contrast agents within plaques. Therefore, combined IVUS/IVPA imaging preserves the ability of conventional IVUS to image the full arterial wall thickness while improving the ability to differentiate plaque composition.

Address all correspondence to: Stanislav Emelianov, University of Texas at Austin, Department of Biomedical Engineering, Austin, Texas 78712. E-mail: emelian@mail.utexas.edu

To date, photoacoustic imaging of arterial vessels has been demonstrated for the localization of endogenous tissues, such as lipid-rich atherosclerotic plaques,[7–12] as well as for the guidance and monitoring of stent placement,[13] and the detection of macrophages labeled with spherical gold nanoparticles.[14,15] Most recently, integrated IVUS/IVPA catheters have been utilized for *in vivo* imaging of human cadavers and live animal models of atherosclerosis for the localization of lipid[11,16] and stents.[17] In the case of *ex vivo* detection of nanoparticle contrast agents, spectroscopic IVPA (sIVPA) imaging was utilized as a means of better differentiating the unique optical absorption spectra of the contrast agents from background tissue. While the labeling of plaque biomarkers with spherical gold nanoparticles, followed by IVUS/IVPA imaging offers the potential for cellular and molecular imaging of atherosclerosis, detection of such contrast agents has not been demonstrated in the presence of luminal blood due to their peak optical absorption occurring within a wavelength region where blood and other endogenous tissues exhibit high optical attenuation and therefore reduce the achievable signal to noise ratio. Therefore, modification of the optical absorption properties of the administered exogenous contrast agents to enable imaging through blood is desirable because it avoids the need for blood removal, a procedure which limits image acquisition time and increases the risk of ischemia and pulmonary edema.[4]

To this end, the current work seeks to extend the use of exogenous contrast agents for IVUS/IVPA imaging to polyethylene glycol (PEG) stabilized gold nanorods (AUNR) with a longitudinal peak absorbance tuned to the near infrared (NIR) wavelength region where blood and endogenous tissues exhibit reduced optical absorption. The conjugation of PEG to AUNR is commonly used as a means of increasing circulation time, reducing cytotoxicity, and preventing aggregation of the nanoparticles.[18] Several groups have recently explored the potential of AUNR as exogenous contrast agents for photoacoustic imaging.[19–21] The current study aims to extend these uses of AUNR to include the selective labeling of atherosclerotic plaque, enabling subsequent detection using combined IVUS/IVPA imaging.

The goal of the current work is to demonstrate that systemically injected AUNR tend to preferentially extravasate at sites of atherosclerotic plaque endothelial dysfunction in rabbit models of atherosclerosis. Subsequently, the high optical absorption of AUNRs within the tissue optical window is utilized to evaluate the ability to detect AUNRs within atherosclerotic plaques in the presence of luminal blood using both single-wavelength and sIVPA imaging. The use of sIVPA, similar to prior work using spherical gold nanoparticle contrast agents, is implemented as a means of differentiating the AUNRs from background tissues. In addition, the use of single-wavelength IVPA imaging at the peak absorption of the AUNRs is also evaluated as a simplified imaging approach capitalizing on the use of a contrast agent which strongly absorbs within the NIR region in which tissue produces a decreased background signal.

## 2  Methods and Materials

### 2.1  *Gold Nanoparticle Preparation*

Cetyltrimethylammonium bromide (CTAB) stabilized AUNRs with an aspect ratio of approximately 3.5 were prepared using a seed mediated growth method.[22] CTAB (Avocado Research Chemicals) was subsequently replaced by 5-kD

molecular weight methoxyl PEG thiol (mPEG-SH, Creative PEGWorks) via ligand exchange to reduce toxicity associated with the cationic CTAB surfactant.[23] Following replacement with PEG, the nanoparticles were washed via centrifugation and resuspended in sterile phosphate buffered saline (PBS) at physiological pH. Figure 1(a) shows the normalized extinction spectra of as prepared CTAB stabilized AUNRs (dotted line), following replacement of the CTAB with mPEG-SH and resuspension in PBS (dash-dotted line), and AUNRs isolated from blood at the time of animal sacrifice (solid line). AUNRs isolated at the time of animal sacrifice show a 20-nm blue shift of the longitudinal absorbance peak relative to the spectrum obtained prior to injection as well as an increased background signal, particularly affecting the transverse peak. Figure 1(b) shows a representative transmission electron microscopy
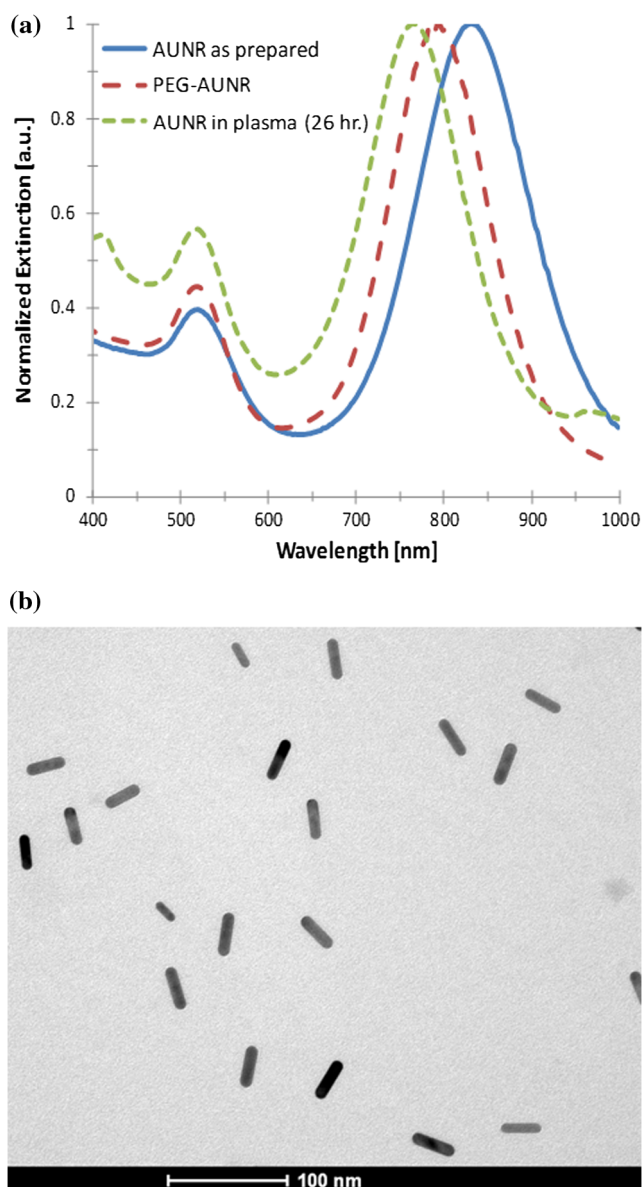




**Fig. 1** Characterization of gold nanorods (AUNRs;color online): (a) extinction spectra of particles as prepared (red), after conjugation of PEG (green), and isolated from blood following rabbit sacrifice (blue). (b) TEM of PEG-AUNR. Scale bar, 100 nm.

(TEM, Tecnai Spirit, FEI Co.) image of PEG-AUNR, revealing monodispersity and no signs of nanoparticle aggregation.

## 2.2 Animal Models of Atherosclerosis

Two distinct rabbit models of atherosclerosis were utilized for this study. For the first model, a New Zealand white (NZW) rabbit was fed a high cholesterol (0.5%) chow diet for 25 days prior to being subjected to balloon injury within the thoracic aorta in order to induce endothelial denudation and inflammation. Following the balloon injury procedure, the rabbit was continued on the high cholesterol chow diet for an additional eight months prior to nanoparticle injection and *ex vivo* imaging. The second atherosclerotic animal model utilized the Watanabe heritable hyperlipidemic (WHHL) rabbit. Due to a deficiency of LDL receptors, WHHL rabbits develop hypercholesterolemia and advanced atherosclerotic lesions on a normal chow diet over the course of one to two years.[24]

## 2.3 In-Vivo Injection of Nanoparticles and Preparation of Tissue Samples

PEG-AUNRs (100 mg, O.D. 200) were injected into the rabbit ear vein and allowed to circulate for 26 h, after which the animal was sacrificed and the aorta was harvested for *ex vivo* imaging. At the time of sacrifice, a blood sample was also taken to determine the absorption spectra of the PEG-AUNRs in order to determine the wavelength of peak absorption for IVPA imaging. Specifically, 5 mL of blood were centrifuged at 1000g for 5 min, and the extinction spectrum of the plasma was measured using a spectrophotometer (BioTek Instruments, Inc.).

The excised aorta was maintained at 4°C, and wrapped in saline-dampened gauze to allow imaging of fresh, unfrozen, tissue for up to 48 h following euthanization of the animals. After imaging, the tissue was fixed in 10% formaldehyde to allow for histological analysis and additional imaging of fixed tissue.

## 2.4 Ex-Vivo Imaging Setup

A schematic diagram of the imaging setup used for IVUS/IVPA imaging with a previously reported integrated catheter is provided in Fig. 2.[25] The output of a tunable OPO laser (SpectraPhysics Inc.) capable of producing 5-ns pulses at 10 Hz with a spectral bandwidth of 2 to 3 nm at NIR wavelengths was coupled to an optical fiber with a core diameter of 600 $\mu$m. The distal tip of the optical fiber was polished at an angle and positioned within a gas-trapping cup to produce side-projecting illumination and this distal housing was coupled to
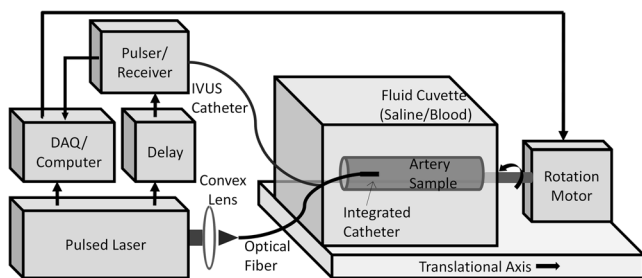


**Fig. 2** Schematic representation of experimental setup for spatially co-registered ultrasound and photoacoustic imaging of *ex vivo* arterial samples using an integrated intravascular ultrasound and intravascular photoacoustic (IVUS/IVPA) catheter.

a commercially available, single element 40-MHz IVUS imaging catheter (Atlantis™ SR plus, Boston Scientific, Inc.), resulting in overlapping ultrasound and optical beams within the aorta lumen.[26] Due to the geometry of the optical fiber and ultrasound transducer, the optical path length through saline or blood is approximately 1 mm less than the ultrasound path length. With each laser pulse, the radio frequency IVPA signals were collected using the IVUS imaging catheter and digitized using a data acquisition (DAQ) card with a sampling rate of 200 MHz (CompuScope 14200, GaGe Applied Technologies, Inc.). Following the triggering of each optical pulse, a user-defined delay of 9 $\mu$s was implemented (DPR-2515, Directed Energy, Inc.) after which an ultrasound pulser-receiver (5073PR, Panametrics-NDT, Inc.) was triggered to transmit an ultrasound pulse with subsequent receiving of an echo signal by the IVUS transducer.

The aorta sample, placed in a cuvette filled with either saline or blood, was secured to rotational and translational stepper-motors (T-LSR150A, Zaber, Inc.), allowing for generation of cross-sectional two-dimensional (2-D) images and three-dimensional (3-D) pullback images, respectively. Each 2-D image consisted of 256 spatially co-registered IVUS/IVPA A-lines per rotation of the aorta sample. Four A-lines were averaged at each position prior to rotation. In the case of 3-D pullback data acquisition, a rotation was performed to generate a 2-D cross-sectional image, followed by translation of the aorta with a step size of 500 $\mu$m.

The *ex vivo* imaging setup allowed for imaging though saline as well as through blood. For imaging performed through blood, human hematocrit (The Blood Center of Central Texas, Austin, TX) was diluted back to the physiological concentration based on a packed cell volume of approximately 40% using saline. The blood was resuspended and added to the cuvette containing the artery section immediately prior to imaging in an effort to minimize denaturing or coagulation of red blood cells within the solution. Additionally, in the case of 3-D IVUS/IVPA imaging through blood, a centrifugal fluid pump was incorporated with the outlet aligned to produce continuous luminal blood flow through the aorta section to reduce ultrasound speckle from blood stasis.

## 2.5 Image Processing Algorithms

Prior to each experiment, the output energy of the illumination fiber was calibrated by adjusting the Q-switch delay to maintain an equal energy at each wavelength to be used for imaging. A beam splitter was positioned proximal to the fiber coupler to deflect a portion of the beam to a power meter (Ophir Optronics Ltd). A look-up table was generated to relate the distal output energy to the measured energy at the position of the power meter. Due to the proportional relationship between local fluence and photoacoustic pressure, variations in the laser output energy can significantly impact the detected IVPA signal. During imaging, the energy of each pulse was recorded and subsequently used to normalize the IVPA signal to account for variation in illumination intensity.

Following normalization for pulse-to-pulse energy variations, IVPA signals over a fixed distance from the integrated catheter were masked-out (i.e., set to zero) to eliminate the effect of ringdown artifacts produced by direct excitation of the IVUS transducer by optical pulse reflection from tissues. Additionally, the intensity of each spatially co-registered IVUS image was used to generate a binary mask of the arterial wall where regions prior to and beyond the arterial wall were set to zero. This binary

mask was then applied to the spatially co-registered IVPA signal to eliminate photoacoustic artifacts and signals from non-tissue (e.g., tissue holder) structures associated with the experimental setup. In the case of imaging through blood, depth dependent fluence attenuation compensation was performed by assuming a Beer's law attenuation of the illumination intensity with the appropriate wavelength dependent extinction coefficient of the reconstituted human blood, which was measured with the UV-VIS spectrophotometer prior to IVUS/IVPA imaging. A user-defined noise floor was then established for all IVPA images, below which signals were ignored for subsequent signal processing steps. Finally, the IVUS and IVPA signals were scan converted from polar to Cartesian coordinates to obtain the cross-sectional images of the aorta, and, in the case of 3-D pullbacks, the serial cross sections were displayed as a volume rendered image stack.

In addition to single-wavelength imaging at the peak absorption of the AUNRs, imaging of sample arterial cross sections was also performed at multiple wavelengths to enable a sIVPA imaging in order to differentiate IVPA signal which originated from AUNRs from those originating from endogenous absorbers or artifacts. For a given cross section, sIVPA imaging was performed by obtaining IVPA signals from 730 to 830 nm wavelengths in 20-nm increments. A constant optical energy was maintained across all wavelengths by adjusting the laser Q-switch delay. More specifically, prior to imaging, a look up table was created to establish the appropriate delay needed to maintain constant optical output across the desired wavelengths. Furthermore, during imaging, the recorded energy of each pulse was also monitored to verify that the output energy remained constant during sIVPA imaging. The IVPA signals were processed as described above, with an identical noise floor selected across all wavelengths. Prior to scan conversion, the IVPA signals at each pixel of the cross-sectional image were normalized as a function of wavelength and compared to normalized reference spectra of known absorbers suspected within the intravascular environment. The reference spectra considered included the extinction spectrum of the AUNRs isolated from blood at the time of animal sacrifice, the absorbance spectrum of oxygenated hemoglobin, and an artificial uniform spectrum. Figure 3(a) and 3(b) provide a graphical representation of the reference spectra and schematic representation of the IVPA data utilized for sIVPA analysis, respectively. The uniform spectrum was intended to account for IVPA signals which may have originated from artifacts such as ultrasound transducer ringdown or increased subsurface fluence at tissue boundaries. These artifacts are expected to yield wavelength-independent IVPA signals over the wavelength range of interest.

A linear least squares algorithm was then utilized to calculate the relative concentrations of the three reference absorbers (AUNRs, oxygenated hemoglobin and artifacts) at each position within the sIVPA image. More specifically, the least squares algorithm is intended to solve for Eq. (1), where the matrix $A$ is composed of the wavelength dependent, normalized absorption coefficients of each of the three reference absorbers, IVPA $(\lambda, i, j)$ is a 3-D matrix composed of the obtained IVPA signals as a function of wavelength ($\lambda$) and position $(i, j)$ and $C(a, i, j)$ represents a matrix of unknown relative concentrations of the references absorbers (a) as a function of position, where $0 \leq C \leq 1$. The unknown relative concentrations $C(a, i, j)$ for the three reference absorbers is obtained by minimizing the squared residuals as expressed in Eq. (2). After computing the matrix $C$, a relative correlation of 0.6 or greater was selected as a threshold for identifying and displaying a pixel containing a particular absorber (e.g., AUNRs).

$$C(a, i, j) \times A(a, \lambda) = \text{IVPA}(\lambda, i, j), \qquad (1)$$

$$\min\{[C(a, i, j) \times A(a, \lambda) - \text{IVPA}(\lambda, i, j)]\}. \qquad (2)$$

## 3 Results

Combined IVUS/IVPA imaging was performed on atherosclerotic rabbit aortas subjected to systemic injection of PEG-AUNR contrast agents approximately 26 h prior to excision of the arteries for *ex vivo* imaging. Results from both a balloon injured NZW rabbit and WHHL rabbit are presented. A representative cross section of the aorta from the balloon injured NZW rabbit model is shown in Fig. 4. Histological staining and dark field microscopy of unstained samples were utilized to evaluate
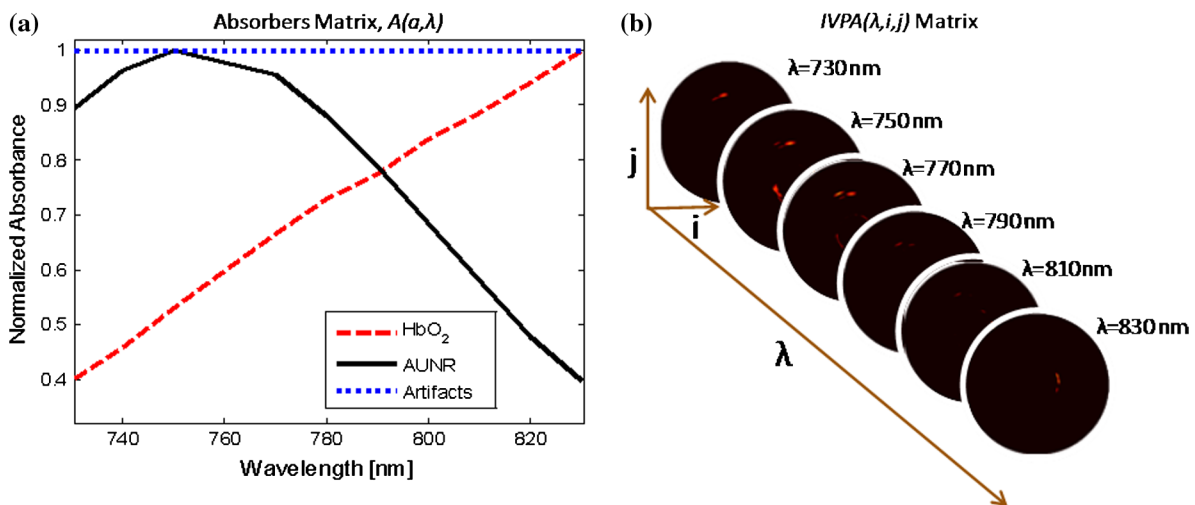


**Fig. 3** Overview of spectroscopic intravascular photoacoustic (sIVPA) image processing system of equations. The absorption spectra of the three reference absorbers were normalized with respect to wavelength (a), and the acquired IVPA signal intensity as a function of position and wavelength (b) was utilized to determine the relative concentration of each reference absorber at each position using a linear least squares algorithm.
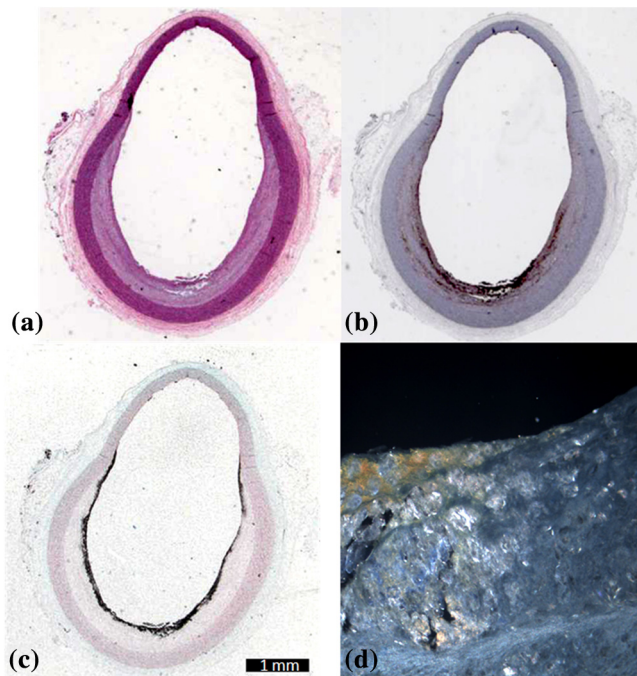
**Fig. 4** Evaluation of gold nanorod (AUNR) labeling of atherosclerotic plaque (color online). Histological staining of adjacent cross sections using (a) hematoxylin and eosin (H&E) for general arterial and plaque morphology, (b) RAM11 stain for labeling macrophages, and (c) silver stain for labeling AUNRs. (d) Representative dark field microscopy image of an unstained artery sections revealing AUNRs (gold color) at the luminal boundary in a region lacking a continuous endothelium or fibrous cap (left), but not in a region with a continuous cap (right). Dark field image obtained using a 20× objective.

the specificity of AUNR labeling to atherosclerotic plaques. Hematoxylin and eosin (H&E) stain shows the presence of an atherosclerotic plaque in the region spanning from 2 to 10 o'clock. RAM11 stain reveals the presence of macrophages near the luminal surface of the plaque. Additionally, dark field microscopy revealed the lack of a healthy endothelial layer at the luminal boundary in plaque regions where AUNRs were present. Furthermore, silver stain histology, used to identify the presence of heavy metals, further indicated the presence of AUNRs near the luminal boundary of the plaque region in agreement with the distribution of macrophages.

Combined IVUS/IVPA imaging was performed on AUNRs-labeled atherosclerotic artery sections in the presence of both luminal saline and luminal blood using the *ex vivo* imaging setup schematically shown in Fig. 2. IVPA and sIVPA images obtained from a sample cross section of a freshly-excised WHHL aorta which was imaged in both saline and blood at 750 nm with output energy of 0.5 mJ are shown in Fig. 5. All IVUS/IVPA images displayed in Fig. 5 represent a total diameter of 22.5 mm, and the optical path length from the integrated IVUS/IVPA catheter to the luminal boundary was measured to range from approximately 2.5 to 5.5 mm. IVPA images are displayed using a 20-dB dynamic range scale [Fig. 5(a), 5(b)]. Silver stain histology from the corresponding cross section is shown in Fig. 5(c). Combined IVUS/sIVPA images display the IVUS signal using a 40 dB dynamic range scale with the regions of spectroscopically detected AUNRs overlaid in green [Fig. 5(d)–5(e)]. Examples of spectroscopic IVPA plots for signals determined to arise from oxygenated hemoglobin

$(HbO_2)$ and AUNRs when imaging through saline and a region identified as containing AUNRs through blood are shown in Fig. 5(f) with the corresponding reference spectra. Errors bars in Fig. 5(f) represent the standard deviation of IVPA signal intensity calculated using a kernel size of approximately 4.5-deg. azimuthal by 55-$\mu$m axial. The plotted spectroscopic response for the AUNR samples was taken from a point near the luminal border at approximately 9 o'clock where the images obtained through both saline and blood show a strong IVPA signal. Contrarily, the sample $HbO_2$ spectroscopic signal was taken from the region in the adventitia at approximately 12 o'clock which was identified as $HbO_2$ by the sIVPA analysis when imaging through saline. Comparison of the single wavelength IVPA and sIVPA signals are in agreement with one another for each imaging environment, saline and blood, as well as with the corresponding silver stain histology [Fig. 5(c)]. Upon evaluation of the 2-D cross section, the IVPA signals obtained at the AUNRs' peak absorbance wavelength (750 nm) show similarly high photoacoustic signals at the 3 and 9 o'clock positions near the position of the arterial wall, which correlate with AUNR accumulation as identified by the silver stain histology image. However, the 12 o'clock position of the IVPA image obtained through blood does not reveal the high intensity signal seen in the case of imaging through luminal saline, and identified as a region with AUNR accumulation in the silver stain histology section. Additionally, the signal-to-noise ratio (SNR) of the image obtained through blood is noticeably reduced in the case of imaging through luminal blood at the same optical fluence. As an example, the SNR of the 9 o'clock region of the IVPA images acquired using at 750 nm excitation through saline and blood were calculated to be approximately 28 and 24 dB, respectively.

Fixed sections of a balloon injured New Zealand white rabbit aorta were subsequently imaged using the integrated IVUS/IVPA catheter. For all combined IVUS/IVPA 3-D renderings shown in Fig. 6, imaging was performed at the AUNRs' peak absorbance wavelength by obtaining full serial cross sections with a step size of 500 $\mu$m. In reconstructing a continuous rendered volume, the combined images were cropped to create a hemispherical view showing the morphology and AUNR distribution within a section of the arterial lumen. A hemispherical view of the IVUS/IVPA signal obtained from imaging an 8-mm arterial section with 0.7-mJ output energy in the presence of saline within the lumen is provided in Fig. 6(a). Following imaging, a digital photograph of the imaged cross section was obtained, revealing the presence and distribution of regions with a high density of AUNRs at the lumen surface, evident by the red color [Fig. 6(b)]. AUNRs visible in the digital photograph are in spatial agreement with regions which provided high signal intensity upon IVPA imaging at the AUNR peak absorbance wavelength. A separate arterial section was then imaged in both saline and blood to further evaluate the potential to detect the AUNRs in the presence of luminal blood using a single optical wavelength. A 6-mm section of the artery was first imaged using the integrated catheter in saline with 0.7-mJ output energy [Fig. 6(c)].The saline was then replaced with the reconstituted human blood, which was pumped through the aorta lumen, and the same cross section was again imaged at the peak wavelength, but with an output energy of 1.4 mJ [Fig. 6(d)]. The similarities of localized IVPA signals obtained through saline and through blood suggest that the AUNRs can be detected through blood.
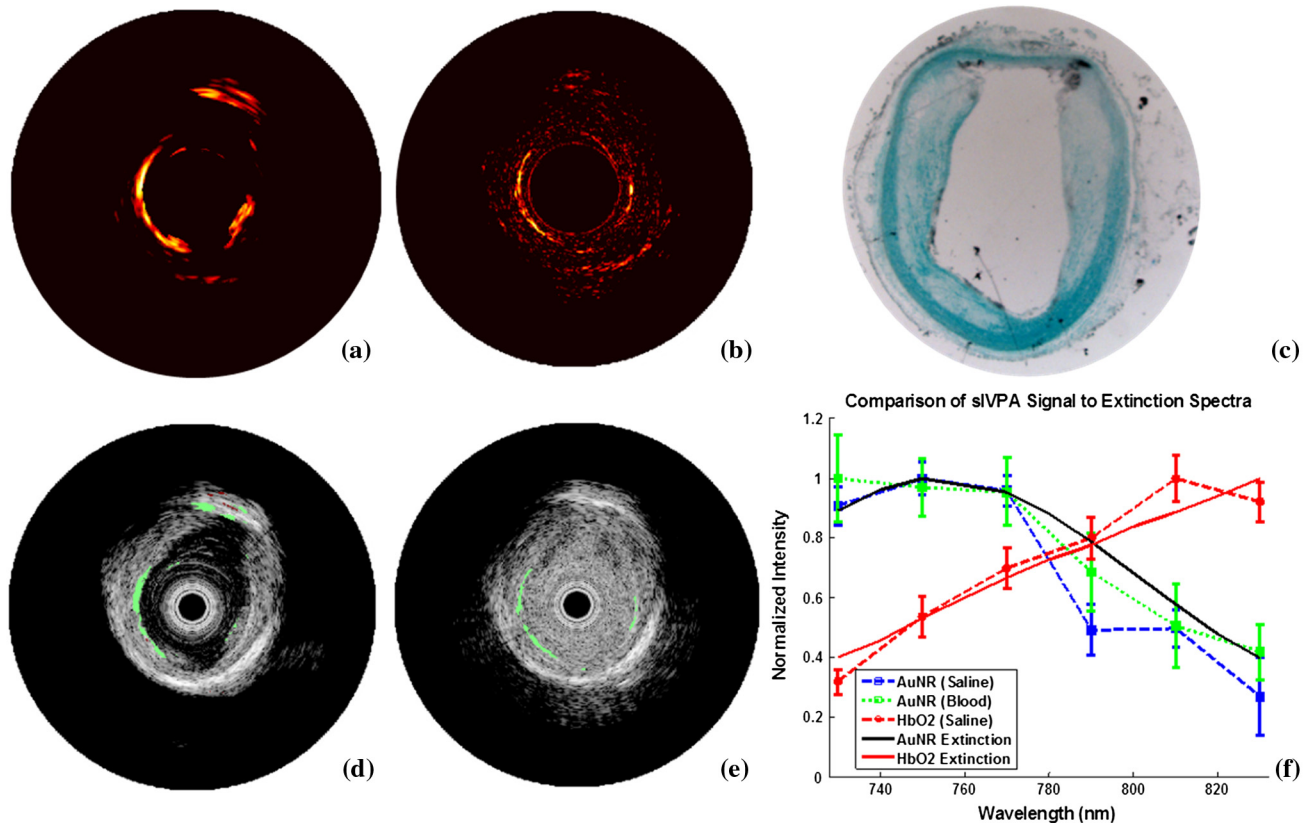
**Fig. 5** Intravascular photoacoustic imaging of gold nanorods (AUNR) labeled atherosclerotic plaque cross section (color online). (a,b) intravascular photoacoustic (IVPA) signal obtained from imaging at the AUNRs peak absorbance wavelength through saline and blood, respectively. Images displayed with 20-dB dynamic range. (c) Corresponding silver stain histology revealing distribution of AUNRs within the plaque. (d, e) Intravascular ultrasound images with overlay of spectroscopic detection of AUNRs through saline and blood, respectively. (f) Comparison of representative spectroscopic IVPA signals, shown as dashed lines, to normalized extinction spectra of AUNRs and oxygenated hemoglobin (HbO2), shown as solid lines.
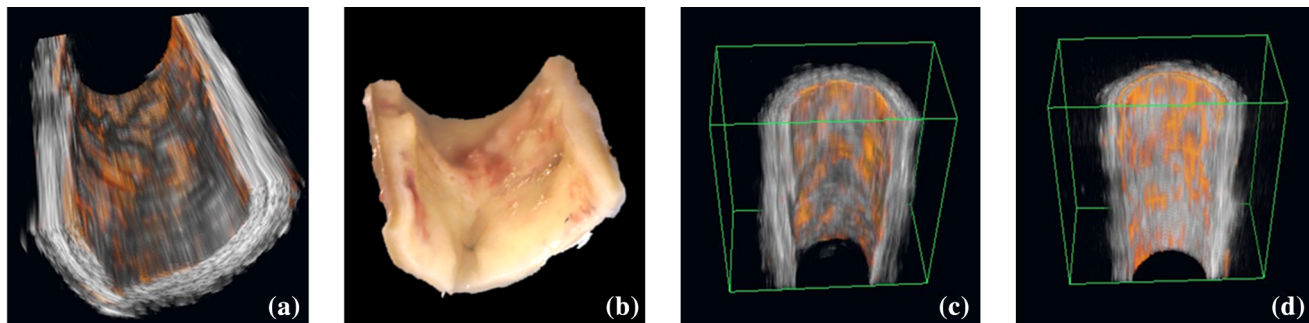


**Fig. 6** Three-dimensional integrated intravascular ultrasound and intravascular photoacoustic (IVUS/IVPA) renderings of gold nanorod (AUNR)-labeled atherosclerotic plaque (color online). (a) Combined IVUS/IVPA rendering of an 8-mm long section of atherosclerotic rabbit artery obtained through saline. (b) Photograph of the corresponding artery section revealing AUNR distribution at the luminal surface (red). Combined IVUS/IVPA images obtained through saline (c), and through blood (d) of aseparate 6-mm arterial section. Step size, 500 $\mu$m.

## 4 Discussion and Conclusions

Gold nanorods conjugated with PEG were investigated as an exogenous contrast agent which preferentially labels sites of atherosclerosis, and which can be localized using combined IVUS/IVPA imaging. Histological staining of sample arterial cross sections was performed to assess AUNR labeling of imaged arterial sections (Fig. 4). AUNR accumulation was limited to the regions of the arterial cross section with atherosclerotic plaque formation [Fig. 4(c)].The nanoparticle labeling is also co-localized with the absence of a healthy, continuous endothelial layer at the lumen boundary [Fig. 4(d)] and the presence of

macrophages [Fig. 4(b)]. While the co-localization of AUNR with macrophages near the luminal boundary is observed, it is unclear whether this co-localization with macrophages is due to phagocytosis of AUNR or if the relationship is the result of a more passive process, such as common sites of extravasation into atherosclerotic plaques.

The correlation between AUNR labeling and missing endothelial or protective fibrous cap layer suggests that the PEG-AUNRs are able to extravasate into the luminal margins of the plaque through discontinuous luminal boundaries. Interestingly, higher magnifications of the silver stain histology

images revealed the presence of AUNRs within the vasa vasorum in the adventitia of regions with atherosclerotic plaque, but not in the regions of a healthy arterial lumen (data not shown). This may also be caused by extravasation through an incomplete endothelial layer, as neovasculature associated with atherosclerosis has been shown to exhibit a leaky endothelium.[27] This hypothesis is further supported by recent reports demonstrating that PEG-AUNRs are not endocytosed by endothelial cells following systemic injection,[28] and that injection of indocyanine green, an organic fluorochrome, resulted in a similar pattern of preferential labeling of atherosclerotic plaques.[29] Furthermore, nanoparticles as larger as 250 nm in diameter have been shown to exhibit selective local permeability due to endothelial barrier disruption in a manner which is related to atherosclerotic severity.[30] Therefore, our results are in agreement with similar studies which have found that systemically injected contrast agents containing no specific biological targeting moiety still tend to preferentially aggregate at atherosclerotic regions and may serve as a tool for assessing plaque vulnerability.

Additionally, the feasibility of detecting AUNR-labeled atherosclerotic plaques was demonstrated through the use of IVPA imaging to detect the location of contrast agents within the context of spatially co-registered IVUS images of arterial morphology. An integrated IVUS/IVPA catheter was utilized to enable imaging in the presence of luminal saline as well as luminal blood in simulated *in vivo* imaging conditions. IVPA imaging of AUNR in the presence of luminal blood is significant in that it simplifies an eventual clinical imaging procedure and avoids potential adverse effects to the patient by eliminating the need for upstream occlusion or saline flushing of the artery.[4] Notably, when the artery sample was imaged in static whole blood, the presence of blood stasis within the lumen of the aorta resulted in significant ultrasound speckle which reduced the ability to detect the arterial morphology [Fig. 5(e)]. The enhanced IVUS speckle has previously been well documented.[31] To reduce this effect and better enable IVUS detection of the arterial wall morphology as is achieved in the case of *in vivo* imaging, a centrifugal pump was positioned to maintain luminal flow while conducting 3-D pullback IVUS/IVPA imaging through blood [Fig 6(d)].

In comparing IVPA images obtained from imaging through luminal saline to those obtained imaging through luminal blood, the similarity of the signals suggests that the relatively low optical attenuation of luminal blood within the NIR wavelength region permits the detection of AUNRs (Figs. 5 and 6). Differences were noted for the cross-sectional image between the 12 o'clock region of the IVPA signal obtained when imaging through saline [Fig. 5(a)] and that achieved through blood [Fig. 5(b)]. Additionally, an overall reduction of the signal-to-noise ratio between the two IVPA signals, obtained using equal catheter output energy of 0.5 mJ, was also observed. Both of these effects are likely due to the increased optical attenuation of blood and can be partially overcome by increasing the delivered pulse energy, as shown in Fig. 6(d).

Notably, when imaging through both saline and blood, the regions which were identified as consisting of AUNR using the sIVPA imaging algorithm are in close agreement with the IVPA signal obtained from imaging only at the AUNR peak absorbance wavelength (Fig. 5). This similarity suggests the potential for localizing accumulated AUNR using combined IVUS/IVPA imaging at a single NIR wavelength rather than across a broad spectral range. This simplification offers the

potential to reduce both image acquisition time and IVPA imaging instrumentation costs. However, further studies should be conducted to quantify the reduction in sensitivity and specificity which result from a single wavelength IVPA AUNR detection approach, particularly as integrated IVUS/IVPA catheter designs continue to evolve and injected AUNR doses are further reduced to become more clinically appealing.

In this study, we demonstrated that PEG-AUNRs preferentially label atherosclerotic regions, and that the AUNRs can be subsequently detected using combined IVUS/IVPA imaging in the presence of luminal blood. Due to the tendency of the AUNRs to extravasate at sites with dysfunctional endothelium, this application of IVPA imaging may be utilized to identify the location of acute inflammation within atherosclerotic plaques, which usually locate within the cap and shoulder regions.[32] In the future, higher aspect ratio AUNRs, which exhibit a longer wavelength longitudinal peak absorbance, as well as the addition of a silica coating, will be investigated as a means of increasing the signal-to-noise ratio and thermal stability of the particles. Additionally, the use of AUNRs can be further expanded to the investigation of molecular IVPA imaging, with the demonstration that the AUNR can be observed in the presence of luminal blood increasing their potential utility for both preclinical and clinical applications in the future. Integration of the presented results demonstrating the ability of combined IVUS/IVPA imaging to localize AUNRs through luminal blood with prior work related to the bioconjugation of targeting moieties to nanoparticle surfaces suggests an avenue for molecular specific IVPA imaging of atherosclerosis biomarkers.

## Acknowledgments

## References

1. L. Roger et al., "Heart disease and stroke statistics-2011 update a report from the American Heart Association," *Circulation* **123**(4), e18–e209 (2011).
2. J. Sanz and Z. Fayad, "Imaging of atherosclerotic cardiovascular disease," *Nature* **451**(7181), 953–957 (2008).
3. B. MacNeill et al., "Intravascular modalities for detection of vulnerable plaque," *Arterioscler. Thromb. Vasc. Biol.* **23**(8), 1333–1342 (2003).
4. K. Hoang et al., "Use of an oxygen-carrying blood substitute to improve intravascular optical coherence tomography imaging," *J. Biomed. Opt.* **14**(3), 034028 (2009).
5. S. Sethuraman et al., "Intravascular photoacoustic imaging using an IVUS imaging catheter," *IEEE Trans. Ultrasonics, Ferroelectr. Freq. Control* **54**(5), 978–986 (2007).
6. S. Sethuraman et al., "Ex vivo characterization of atherosclerosis using intravascular photoacoustic imaging," *Opt. Exp.* **15**(25), 16657–16666 (2007).
7. H. Wang et al., "Label-free bond-selective imaging by listening to vibrationally excited molecules," *Phy. Rev. Lett.* **106**(23), 238106 (2011).
8. T. Allen et al., "Spectroscopic photoacoustic imaging of lipid-rich plaques in the human aorta in the 740 to 1400 nm wavelength range," *J. Biomed. Opt.* **17**(6), 061209 (2012).
9. S. Sethuraman et al., "Spectroscopic intravascular photoacoustic imaging to differentiate atherosclerotic plaques," *Opt. Exp.* **16**(5), 3362–3367 (2008).

10. B. Wang et al., "Detection of lipid in atherosclerotic vessels using ultrasound-guided spectroscopic intravascular photoacoustic imaging," *Opt. Exp.* **18**(5), 4889–4897 (2010).

11. K. Jansen et al., "Intravascular photoacoustic imaging of human coronary atherosclerosis," *Opt. Lett.* **36**(5), 597–599 (2011).

12. B. Wang et al., "Intravascular photoacoustic imaging of lipid in atherosclerotic plaques in the presence of luminal blood," *Opt. Lett.* **37**(7), 1244–1246 (2012).

13. J. Su, B. Wang, and S. Emelianov, "Photoacoustic imaging of coronary artery stents," *Opt. Exp.* **17**(22), 19894–19901 (2009).

14. B. Wang et al., "Plasmonic intravascular photoacoustic imaging for detection of macrophages in atherosclerotic plaques," *Nano Lett.* **9**(6), 2212–2217 (2009).

15. B. Wang et al., "Intravascular photoacoustic imaging of macrophages using molecularly targeted gold nanoparticles," *Proc. SPIE* **7564**, 75640A (2010).

16. B. Wang and B. Wang et al., "In vivo intravascular ultrasound-guided photoacoustic imaging of lipid in plaques using an animal model of atherosclerosis," *Ultrasound Med. Biol.*, in press (2012).

17. A. Karpiouk et al., "Feasibility of in vivo intravascular photoacoustic imaging using integrated ultrasound and photoacoustic imaging catheter," *J. Biomed. Opt.* **17**(9), 096008 (2012).

18. T. Niidome et al., "PEG-modified gold nanorods with a stealth character for in vivo applications," *J. Controlled Release* **114**(3), 343–347 (2006).

19. M. Eghtedari et al., "High sensitivity of in vivo detection of gold nanorods using a laser optoacoustic imaging system," *Nano Lett.* **7**(7), 1914–1918 (2007).

20. P. Li et al., "In vivo photoacoustic molecular imaging with simultaneous multiple selective targeting using antibody-conjugated gold nanorods," *Opt. Exp.* **16**(23), 18605–18615 (2008).

21. A. Taruttis et al., "Real-time imaging of cardiovascular dynamics and circulating gold nanorods with multispectral optoacoustic tomography," *Opt. Exp.* **18**(19), 19592–19602 (2010).

22. N. Jana, L. Gearheart, and C. Murphy, "Seed-mediated growth approach for shape-controlled synthesis of spheroidal and rod-like gold nanoparticles using a surfactant template," *Adv. Mat.* **13**(18), 1389–1393 (2001).

23. C. Grabinski et al., "Effect of gold nanorod surface chemistry on cellular response," *ACS Nano* **5**(4), 2870–2879(2011).

24. M. Shiomi and T. Ito, "The Watanabe heritable hyperlipidemic (WHHL) rabbit, its characteristics and history of development: a tribute to the late Dr. Yoshio Watanabe," *Atherosclerosis* **207**(1), 1–7 (2009).

25. A. Karpiouk, B. Wang, and S. Emelianov, "Development of a catheter for combined intravascular ultrasound and photoacousticimaging," *Rev. Sci. Instrum.* **81**(1), 014901 (2010).

26. A. Karpiouk, B. Wang, and S. Emelianov, "Development of a catheter for combined intravascular ultrasound and photoacoustic imaging," *Rev. Sci. Instrum.* **81**(1), 014901 (2010).

27. R. Virmani et al., "Atherosclerotic plaque progression and vulnerability to rupture: angiogenesis as a source of intraplaque hemorrhage," *Arterioscler. Thromb. Vasc. Biol* **25**(10), 2054–2061 (2005).

28. A. Alkilany et al., "Toxicity and cellular uptake of gold nanorods in vascular endothelium and smooth muscles of isolated rat blood vessel: importance of surface modification," *Small* **8**(8), 1270–1278 (2012).

29. C. Vinegoni et al., "Indocyanine green enables near-infrared fluorescence imaging of lipid-rich, inflamed atherosclerotic plaques," *Sci Transl. Med.* **84**(3), 84 ra45 (2011).

30. H. Zhang et al., "Quantifying the evolution of vascular barrier disruption in advanced atherosclerosis with semipermeant nanoparticle contrast agents," *PLoS ONE* **6**(10), e26385 (2011).

31. G. S. Mintz, "Quantitative and Qualitative Analyses," Chapter 2, in *Intracoronary Ultrasound*, Taylor & Francis, Oxon, UK, pp. 23–25 (2005).

32. G. Pasterkamp et al., "Inflammation of the atherosclerotic cap and shoulder of the plaque is a common and locally observed feature in unruptured plaques of femoral and coronary arteries.," *Arterioscler. Thromb. Vasc. Biol.* **19**(1), 54–58 (1999).